NOTES AND CORRESPONDENCE

Impact of Satellite Winds on Marine Wind Simulations

WILL PERRIE

Fisheries and Oceans Canada, Bedford Institute of Oceanography, Dartmouth, Nova Scotia, Canada

WEIQING ZHANG

Environment Canada, Downsview, Ontario, Canada

MARK BOURASSA

Center for Ocean–Atmospheric Prediction Studies, The Florida State University, Tallahassee, Florida

HUI SHEN

Fisheries and Oceans Canada, Bedford Institute of Oceanography, Dartmouth, Nova Scotia, Canada, and Institute of Oceanology, Chinese Academy of Sciences, Qingdao, China

PARIS W. VACHON

Defence R&D Canada, Ottawa, Ontario, Canada

(Manuscript received 13 October 2006, in final form 7 August 2007)

ABSTRACT

A variational data assimilation method is applied to remotely sensed wind data from Hurricanes Gustav (2002) and Isabel (2003) to produce enhanced marine wind estimates. The variational method utilizes constraints to ensure that an optimum combination of winds is determined, in the sense of minimization of a cost function measuring the misfit between observations and background input field data and constraining nongeophysical features in the spatial derivatives. Constraints are multiplied by weights, which are objectively determined by cross validation. Verification is obtained by comparison with available operational in situ buoy observations and analyses winds. It is shown that the newly constructed midlatitude wind fields represent an improvement relative to background wind field estimates and also relative to Quick Scatterometer–National Centers for Environmental Prediction reanalysis blended winds, and that the new winds have an impact on simulations of waves and upper-ocean currents.

1. Introduction

High winds and waves frequently occur in North Atlantic Ocean waters, particularly with the generation and development of hurricanes. For example, in September 2002 Hurricane Gustav tracked past Nova Scotia, between Sable Banks and the mainland shoreline, as a category-2 hurricane. In September 2003, Hurricane Isabel developed to category-5 intensity north of the Caribbean and, moving toward the northwest, weakened to category 2 as it made landfall in North Carolina. Collecting detailed information about the high-wind regions of hurricanes is often difficult and constitutes an important limitation on accurate estimates for ocean waves and currents. Satellite data have proven to be valuable because of their ability to achieve large spatial coverage and high resolution. Among spaceborne sensors, synthetic aperture radar (SAR) and microwave scatterometer can penetrate clouds and (to some extent) rain, and accurately mea-

Corresponding author address: William Perrie, Bedford Institute of Oceanography, 1 Challenger Dr., P.O. Box 1006, Dartmouth, NS B2Y 4A2, Canada.
E-mail: perriew@dfo-mpo.gc.ca

DOI: 10.1175/2007WAF2006093.1

sure the ocean surface, even in severe weather conditions.

An objective of this note is to demonstrate a variational technique to combine satellite and numerical weather prediction (NWP) wind data. To construct high-quality marine wind estimates in Hurricane Gustav, we first generated NWP winds using the Canadian Meteorological Centre (CMC) Mesoscale Compressible Community (MC2) atmospheric model (Benoit et al. 1997). We then applied a variational data assimilation method (Pegion et al. 2000; O'Brien and Bourassa 2003; Bourassa et al. 2002; Morey et al. 2005) to combine all available coincident scatterometer data (archived at a 12-h interval centered on the analysis time) from Quick Scatterometer (QuikSCAT; also denoted QSCAT) and NWP model outputs. The resultant maximum winds are shown to compare more favorably to National Hurricane Center (NHC) winds than do the QSCAT–National Centers for Environmental Prediction (NCEP) analyses winds (information online at http://dss.ucar.edu/datasets/ds744.4/), which are obtained by blending QSCAT data with NCEP reanalysis winds (Chin et al. 1998). The NHC method is described by Powell et al. (1998). Wind field errors lead to errors in simulations of waves and ocean surface currents. In simulating Gustav, our new enhanced winds are used to drive models for waves and ocean currents, and the results are shown to compare favorably to observations collected along Gustav's storm track as it passed by Nova Scotia.

A related objective of this note is to show that synthetic aperture radar (SAR) derived winds can result in improved marine wind estimates. For hurricane Isabel, we focus on *Radar Satellite-1* (*RADARSAT-1*) SAR wind data and construct marine wind estimates by using the variational method to combine SAR data with background fields consisting of QSCAT, QSCAT–NCEP, and CMC analysis wind data. A heavy assimilation weight was used for SAR data. Winds are derived from SAR using a hurricane wind retrieval algorithm developed by Shen et al. (2006). This method uses the C-band geophysical model function 5 (CMOD5) geophysical model function (Hersbach 2003) following Horstmann et al. (2005). In applying CMOD5 to horizontal polarized *RADARSAT-1* SAR images, we used a hybrid model suggested by Thompson et al. (1998) with polarization ratio parameter $\alpha = 1$, as suggested by Vachon and Dobson (2000). Recently, Mouche et al. (2006) have suggested that the polarization ratio has an azimuthal dependence. Our resultant winds are shown to compare more favorably to NHC winds than what is achieved with QSCAT–NCEP winds.

Section 2 describes models used in this study, and section 3 discusses the satellite data. Descriptions of Hurricanes Gustav and Isabel are given in section 4, and wind and upper-ocean results appear in sections 5 and 6. Conclusions are summarized in section 7.

2. Model descriptions

The MC2 model is a state-of-the-art, fully elastic, nonhydrostatic model solving the full Euler equations on a limited-area Cartesian domain. Semi-Lagrangian advection and a semi-implicit time-differencing dynamic scheme allow MC2 to be able to successfully simulate midlatitude cyclones (Benoit et al. 1997). The Kain–Fritsch scheme (Kain and Fritsch 1993) is used for deep cumulus convection, as well as related boundary layer, turbulent kinetic energy (TKE), and vertical diffusion parameterizations (Benoit et al. 1997). Lateral boundary and initial conditions are taken from the CMC analysis data. For Gustav simulations, the model domain is (24.25°–56.25°N, 79.5°–40.0°W), using a latitude–longitude projection, 0.25° resolution, 30 vertical layers, and 600-s time steps. Surface heat and moisture fluxes over land are calculated from a force–restore scheme (Benoit et al. 1997). Over the sea, MC2's interfacial fluxes of momentum and sensible and latent heat are calculated using Monin–Obukhov theory. For a complete description of the model dynamics, the reader is referred to Benoit et al. (1997).

The Princeton Ocean Model (POM) by Mellor (1998) is implemented on a latitude–longitude projection (20°–57.5°N, 82°–40°W), with 0.16° horizontal resolution and 23 vertical layers, of which 8 are in the upper 80 m. Lateral prescribed barotropic transports are used to keep the Gulf Stream in the right position. Initial and boundary conditions for temperature and salinity are taken from monthly Naval Oceanographic Office Generalized Digital Environmental Model (GDEM) data (Bender and Ginis 2000).

The WAVEWATCH III (WW3) ocean wave model (Tolman 2002; Tolman et al. 2002) is implemented on the same domain as the MC2 model, also with 0.25° resolution. The model simulates directional wave spectra in terms of wavenumber-direction bands by solving the well-known spectral action balance equation for waves. WW3 has been shown to perform well in simulations of observed hurricane-generated waves for a variety of storms (Moon et al. 2003; Xu et al. 2007).

The variational method was first developed for daily National Aeronautics and Space Administration (NASA) Scatterometer (NSCAT) observations (Pegion et al. 2000) and then was modified for monthly in situ winds and fluxes (Bourassa et al. 2005) and for

fine-resolution episodic forcing (Morey et al. 2005, 2006). The objective technique minimizes a cost function [Eq. (1)], which balances (through soft constraints) reduction of (a) the misfit to observations with (b) the misfit to vorticity of a background field and (c) smoothing with respect to the background field. The weights for each of these terms are objectively derived by a cross-validation method. This technique removes observations from the input to the cost function and determines the weights by the insensitivity of the removed observations to the output field (Pegion et al. 2000).

The functional f, given by

$$f = \sum_{i,j}^{I,J} \{\beta_a \sigma_{P_o}^{-2}[(P_x - P_{x_{o1}})^2 - (P_y - P_{y_{o1}})^2] + \beta_b \sigma_{P_o}^{-2}[(P_x - P_{x_{o2}})^2 - (P_y - P_{y_{o2}})^2] + \beta_c L^4[\nabla^2(P_x - P_{x_{\mathrm{bg}}})]^2 + \beta_c L^4[\nabla^2(P_y - P_{y_{\mathrm{bg}}})]^2 + \beta_d L^2[k \cdot \nabla \times (\mathbf{P} - \mathbf{P}_{\mathrm{bg}})]^2\}, \quad (1)$$

is minimized to find the solution pseudostress (P_x, P_y), which is the product of the wind vector and speed. The terms with the "o" subscripts are satellite observations averaged with a grid cell ($o1$ for QSCAT, and $o2$ for SAR), and the terms with the "bg" subscripts are the background field. The β terms are weights, σ is the uncertainty of the observational average within a grid cell, and L is a grid-spacing-dependent dimensionless length scale. The first terms (β_a and β_b weights) represent the misfits to the satellite observations, the second term (β_c weights) is a penalty function to smooth each vector component with respect to the background field, and the last term (β_d weights) is a misfit to the vorticity of the background field.

Previous operational QSCAT gridded wind products produced through this technique have used background fields constructed from 3-day binned QSCAT wind data, Gaussian smoothed over a 5° radius, where these scales represent three standard deviations in the Gaussian distributions. Alternatively, a blended NWP and QSCAT product has been created by replacing the background with either Eta-29 or NCEP wind fields (Morey et al. 2005), or with a weighted blend of QSCAT, NCEP, and NOAA/NHC/Hurricane Research Division (HRD) hurricane wind analysis (H*WIND) fields (Morey et al. 2006). The blended QSCAT and NWP approach, when applied to episodic forcing, is much better than either NWP or QSCAT alone. Herein, the background is based on a blending of NWP and QSCAT data. The key difference from previous efforts is the SAR data in the misfit to observations for Isabel.

3. Satellite data

In this study, scatterometer winds are daily, gridded SeaWinds on the QSCAT level-3 system. The system measures winds between 3 and 30 m s^{-1} with an accuracy better than (the greater of) 2 m s^{-1} or 10% in speed and 20° in direction with a spatial resolution of 25 km. QSCAT accuracy has typically been assessed through root-mean-square (RMS) difference calculations involving various sets of comparison data (NWP models, other satellite winds, buoys, and research vessels). These comparisons apply only to rain-free observations. In such comparisons (e.g., Ebuchi et al. 2002), the RMS differences are typically about 1 m s^{-1} in speed, with 0.6 m s^{-1} uncertainty for QSCAT vector components (M. Freilich and A. Stoffelen 2002, personal communication). A comparison that considers spatial and temporal mismatches results in substantially lower (but less statistically robust) uncertainty estimates (Bourassa et al. 2003).

One of the limitations of scatterometers is that wind estimates are contaminated by heavy rain. This is caused by attenuation (reduction) of the signal as it travels to and from the ocean surface, an increased signal due to backscatter from the raindrops, and increased sea surface roughness caused by raindrop splashing on the ocean surface. For light wind conditions, heavy rain causes an overestimate of the wind speed, due to increased backscatter from the raindrops and increased roughness caused by splashing on the ocean surface. Conversely, rain contamination has less effect on wind speed estimates in stronger wind situations since the increased sea surface roughness caused by the wind dominates over the rain effect. The QSCAT rain flag was originally designed to flag all wind vectors that might be influenced by rain. Subsequently, Weissman et al. (2002) and Draper and Long (2004) found that rain caused substantial ill effects only if the rain rate was greater than a wind speed–dependent threshold.

Because rain contamination is severe when the rain-related signal is similar to (or greater than) the signal from the wind roughening of the surface, serious problems often occur for strong tropical storms, but they are less serious for subtropical and extratropical cyclones, which usually have smaller rain rates. In tropical

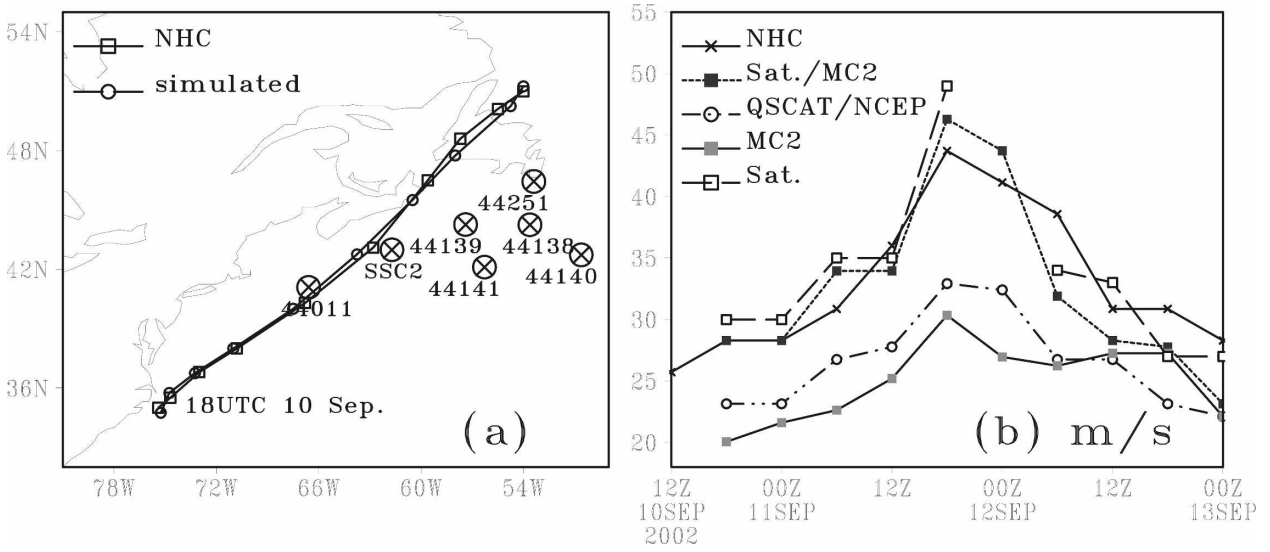

FIG. 1. (a) Comparison of storm track from NHC and MC2 simulations, showing buoy locations for wind and wave observations (labeled 44xxx) and current measurements at SSC2. (b) Maximum 10-m winds (m s^{-1}) following the storm trajectory starting at 1800 UTC 10 Sep 2002, including QuikSCAT data alone (labeled Sat.); baseline MC2 winds; QSCAT–NCEP winds; our Sat–MC2 winds, which blend QuikSCAT and MC2 winds; and NHC winds. All winds are reduced to 10-m reference level by using the neutral logarithmic wind law.

storms, the rain signal often exceeds the wind signal, resulting in severe problems in wind retrievals. For extratropical hurricanes, the wind signal increases (relative to tropical storms) more than does the rain signal. In many cases the extratropical hurricane wind signal exceeds the rain signal, so the rain contamination often leads to relatively small errors; whereas for tropical storms, the errors are often very large, particularly in wind direction. Consequently, QSCAT observations are more reliable for these storms. Rather than apply a rain flag that is ill-designed for our application, a filter is applied to remove observations that depart more than three standard deviations from a local mean, where the mean and standard deviation have been determined from observations within a 3×3 gridcell area. The filter eliminates the majority of observations with substantial rain-related errors, regardless of whether or not they were rain flagged.

C-band SAR data are less affected by rain than Ku-band scatterometer data. Rain effects related to SAR are discussed by Alpers and Melsheimer (2004). High spatial resolution (i.e., kilometer scale) wind fields may be derived from SAR imagery by using the observed radar backscatter, the SAR geometry, an estimate of the wind direction, and a geophysical model function that applies to the radar frequency and polarization (C-band and HH polarization for *RADARSAT-1*). The difficulty in determining winds from SAR is usually associated with finding an appropriate wind direction estimate, either from the SAR image itself, or other wind estimates, or through variational methods. For wind retrieval from *RADARSAT-1*, using wind directions from collocated buoy observations, the retrieved winds were shown to be within ± 2.4 m s^{-1} of the buoy wind speed, for winds up to 20 m s^{-1} (Vachon and Dobson 2000). Other validation data sources and geophysical model functions give similar or better wind retrieval accuracy and may have better performance at higher wind speeds (Horstmann et al. 2005).

4. Storm cases

Hurricane Gustav was designated a tropical storm by 1200 UTC on 10 September 2002, north of the Bahamas. Nearing Cape Hatteras on 11 September, it turned northeastward and accelerated, embedded within a southwesterly flow ahead of a midlevel trough centered on New England. Dominated by baroclinic processes, Gustav intensified rapidly over 28°C Gulf Stream waters and began to merge with the associated midlatitude low. Gustav became a hurricane by 1200 UTC, with maximum winds of 85 kt (43 m s^{-1}) near 1800 UTC. It made landfall over Cape Breton with 80-kt winds, achieving minimum central sea level pressure (SLP) at 0600 UTC 12 September. It made a transition to an extratropical cyclone and, turning north, made a second landfall over Newfoundland.

Hurricane Isabel originated in the central Atlantic Ocean on 6 September 2003. It intensified to a category-5 storm and moved westward, north of the Caribbean and Bahamas. On 14 September, Isabel's

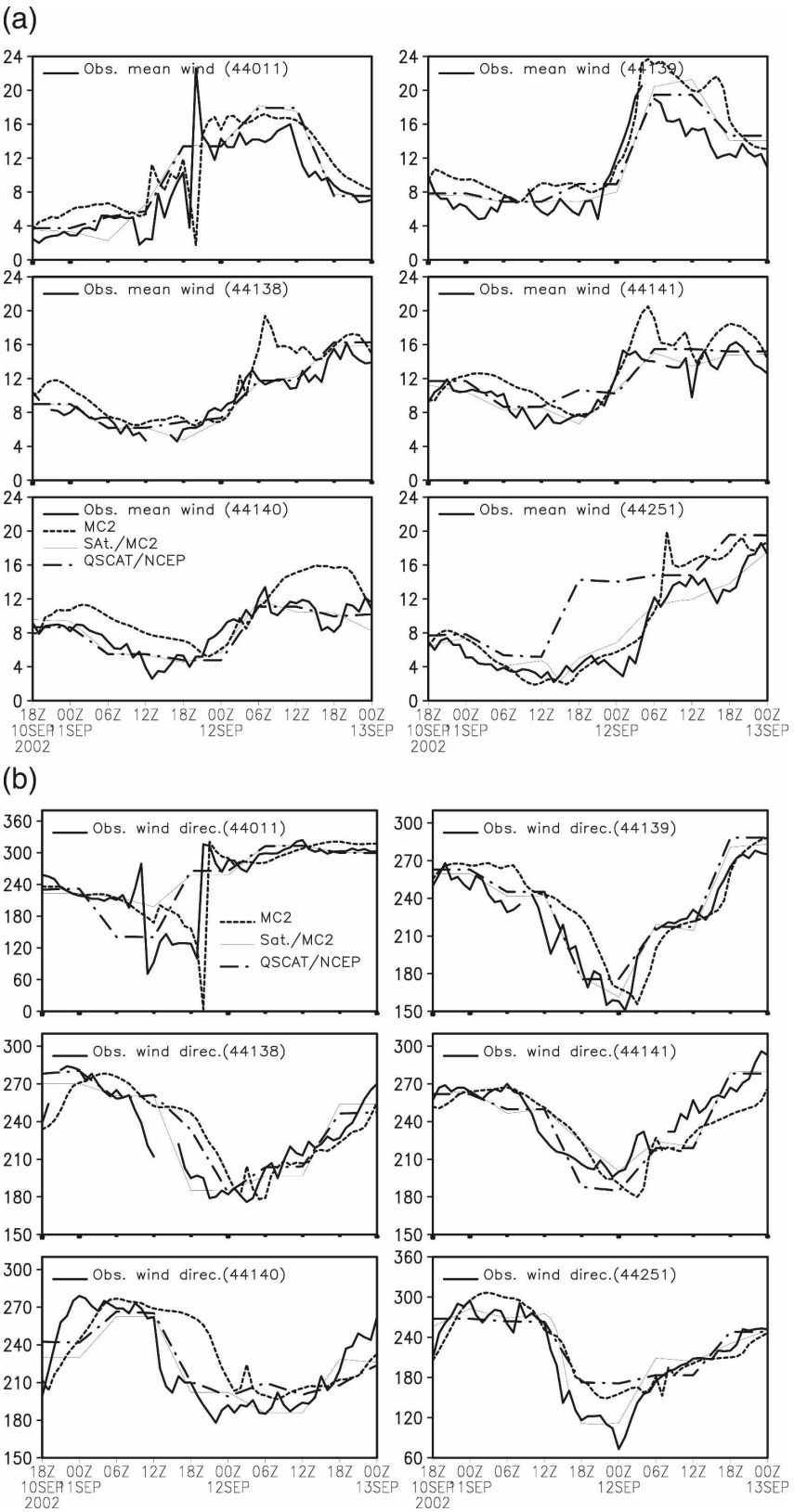

FIG. 2. (a) Wind speed (m s^{-1}) at buoy locations (see Fig. 1a) in comparison with baseline MC2 winds, Sat–MC2 winds, and QSCAT–NCEP winds. (b) As in (a) but for wind direction (°).

movement slowed, after turning toward the northwest. Cooler waters over which it passed prevented further intensification. It continued to weaken as it headed toward the North Carolina coast, making landfall as a category-2 storm at Ocracoke Island between Cape Hatteras and Cape Lookout, with maximum sustained winds near 85 kt around 1700 UTC 18 September.

5. Marine wind simulations

a. Hurricane Gustav

The storm track for Hurricane Gustav is shown in Fig. 1a, as estimated by the baseline MC2 simulation (also denoted NWP), and compares well to the NHC estimates. The model integration (in Fig. 1a) is from 1800 UTC 10 September to 1200 UTC 13 September. Gustav moved slowly during the initial portion of the simulations, and accelerated during its extratropical phase as it moved past Nova Scotia. Figure 1a also gives locations for in situ measurements of wind, waves, and currents. The time series of peak storm winds from MC2 estimates are shown in Fig. 1b, following the storm trajectory, in comparison with QSCAT, NHC, and QSCAT–NCEP winds. Figure 1b shows that the MC2 winds are comparable to QSCAT–NCEP winds and fail to capture the intensity of the NHC winds. The bias in these two wind estimates is as much as 12 m s^{-1} at the peak of the storm, relative to NHC. The QSCAT winds (values on 0000 UTC 12 September) tend to be slightly higher than NHC winds before 1800 UTC 11 September, and lower afterward. By comparison, our variational blending of MC2 winds and scatterometer data (denoted Sat/MC2) gives results that are similar to NHC winds and that improve on MC2 estimates.

Time series comparisons of wind speed and direction at buoy locations (see Fig. 1a), at various distances from the storm center are shown in Figs. 2a and 2b. There is a systematic trend that suggests that our enhanced Sat–MC2 winds are an improvement relative to baseline MC2 winds. Statistical measures of this improvement in terms of correlation coefficients and root-mean-square errors (RMSE) are given in Table 1. Our Sat–MC2 winds have an average RMSE of 1.89 m s^{-1}, as compared with average RMSEs of 3.1 m s^{-1} for baseline MC2 winds and 2.58 m s^{-1} for QSCAT–NCEP. This is much smaller than the differences evident in Fig. 1b, where maximum winds from Sat–MC2 are clearly more comparable to NHC winds than to QSCAT–NCEP winds. We obtained this result because the buoys are outside of the main high-wind area, as shown by the relatively low winds they report and the relatively small differences between the QSCAT–NCEP and Sat–MC2 winds.

TABLE 1. Correlation coefficients and RMSE for 10-m winds between observations and the uncoupled MC2 control simulation, the blended Sat–MC2 wind, and the blended QSCAT–NCEP wind. Buoy locations are given in Fig. 1a.

Buoy	44011	44138	44139	44140	44141	44251
			Correlation coef			
MC2	0.7461	0.8806	0.8925	0.6604	0.8832	0.9562
Sat–MC2	0.8646	0.9501	0.8784	0.8466	0.8902	0.9535
QSCAT–NCEP	0.8783	0.9436	0.8809	0.8528	0.8185	0.7665
			RMSE			
MC2	4.0185	2.6381	3.6771	3.3295	2.6141	2.3011
Sat–MC2	3.0178	1.1673	2.7034	1.4324	1.3551	1.6793
QSCAT–NCEP	2.8890	1.2393	2.5426	1.4435	1.9526	5.4268

Figures 3a–d compare the spatial distribution of QSCAT–NCEP analysis winds (0.5° resolution) with our Sat–MC2 winds (0.5° and 0.25° resolutions). Although the figures are qualitatively similar, notable differences occur in the structure and the peak wind regions between the QSCAT–NCEP winds and the Sat–MC2 winds (comparing the 0.5°-resolution plots). A dipole structure is exhibited in the peak wind difference field (Fig. 3d) with a maximum of about 12 m s^{-1} indicating differences in the locations of the peak wind regions. Differences can be attributed to background data in the region of the storm peak (MC2 or global NCEP reanalysis data) or to different assimilative methods. This is clear because the assimilated scatterometer data are the same in both plots, and outside the maximum wind regions, the QSCAT–NCEP and Sat–MC2 winds are qualitatively similar, for both 0. 5° and 0.25° resolutions (Figs. 3a–c).

b. Hurricane Isabel

Figures 4 and 5 present wind speed contours and vectors for Hurricane Isabel, as well as locations of two National Data Buoy Center (NDBC) buoys, which recorded wind data. Winds from QuikSCAT data for all swaths during the period from 0600 to 1800 UTC 18 September 2003 are given in Figs. 4a and 5a (at 0.25° resolution). Using background data consisting of 1) 12 h of available QuikSCAT data centered on the analysis time 1200 UTC 18 September 2003 and 2) QSCAT–NCEP data at 1200 UTC 18 September 2003 (which are used to fill in the gaps between the QuikSCAT swaths), we used our variational method to assimilate the SAR-observed data. The SAR wind field for this time period occurs at 1100 UTC 18 September (shown in Figs. 4b and 5b) and is derived following the new algorithm of Shen et al. (2006). Corresponding QSCAT–NCEP winds (with 0.5° resolution) are shown in Figs. 4c and 5c. The SAR image completely covers the eye of Isabel

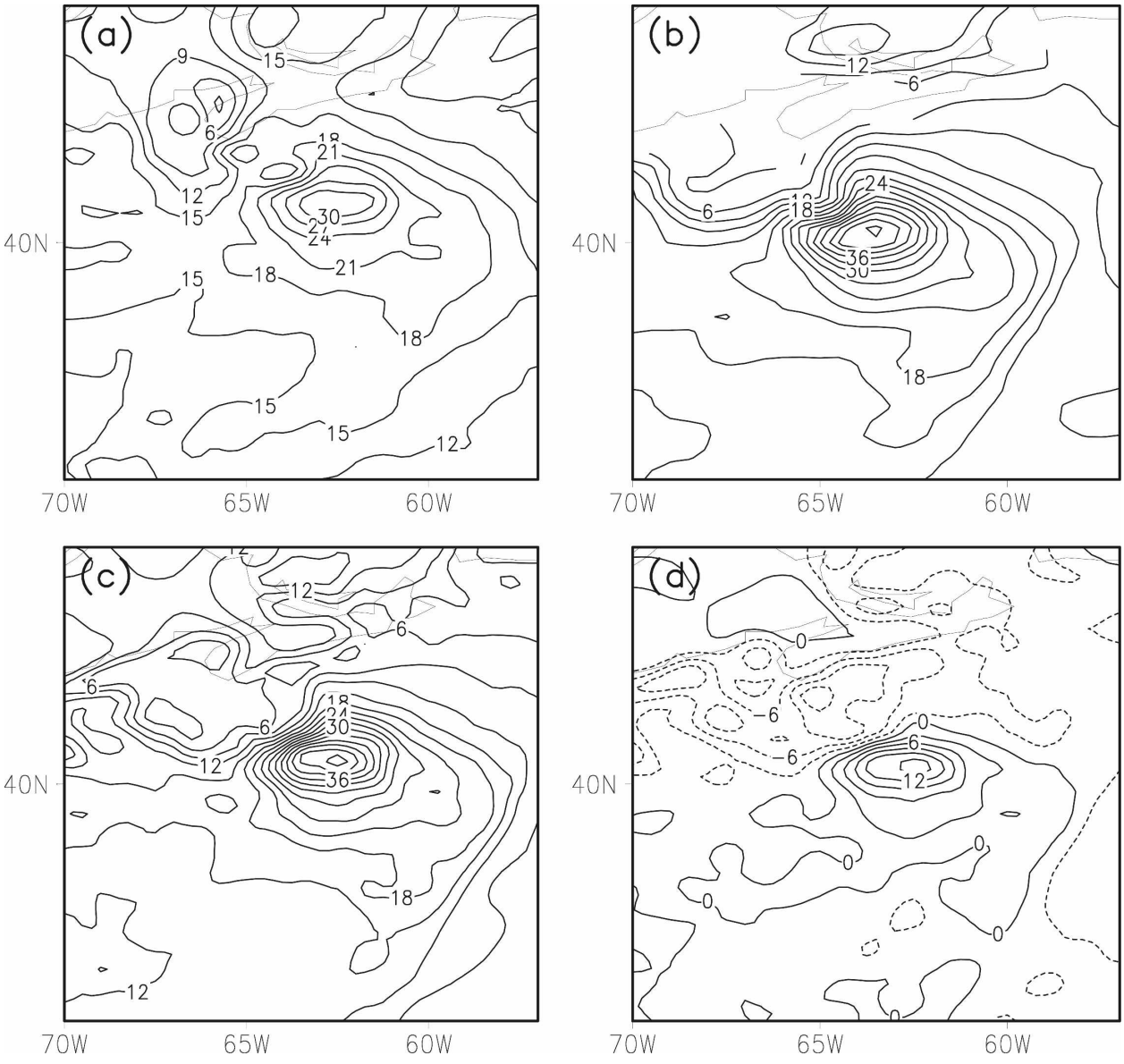

FIG. 3. Wind speed (m s^{-1}) (a) from QSCAT–NCEP with 0.5° resolution at 1800 UTC 11 Sep 2002, (b) from Sat–MC2 with 0.5° resolution, and (c) from Sat–MC2 with 0.25° resolution, and (d) the difference in the Sat–MC2 winds in (b) *minus* the QSCAT–NCEP winds in (a). Maximum wind is about 30 m s^{-1} in (a) and 42 m s^{-1} in (b) and (c), and the maximum difference is about 12 m s^{-1} in (d).

and suggests details not evident in the QuikSCAT images. Our resulting blended winds appear in Figs. 4d and 5d (with 0.25° resolution). These results are relatively insensitive to the influence of resolution and when we use QuikSCAT winds at 0.5° resolution (Fig. 4e) we obtained results similar to those shown in Fig. 4f.

In terms of background fields, we also tried filling the gaps between QuikSCAT swaths with CMC winds, or alternately QuikSCAT data, by including swaths over an extended time, ±15 h centered on the analysis time. In either case, the resulting winds were essentially the same as in Figs. 4d and 5d, which use QSCAT–NCEP data to fill the QuikSCAT gaps. These results occur because the central region of the storm is in fact covered by the QuikSCAT swaths, and although QSCAT–NCEP data may significantly differ from QuikSCAT or CMC data in this region, these wind maps are all very similar in less rapidly varying regions of the storm that constitute the swath gaps. Moreover, ascribing heavy assimilation weights to SAR data allows the SAR image to dominate the assimilative blending, and the SAR images captured the central eye region of Isabel.

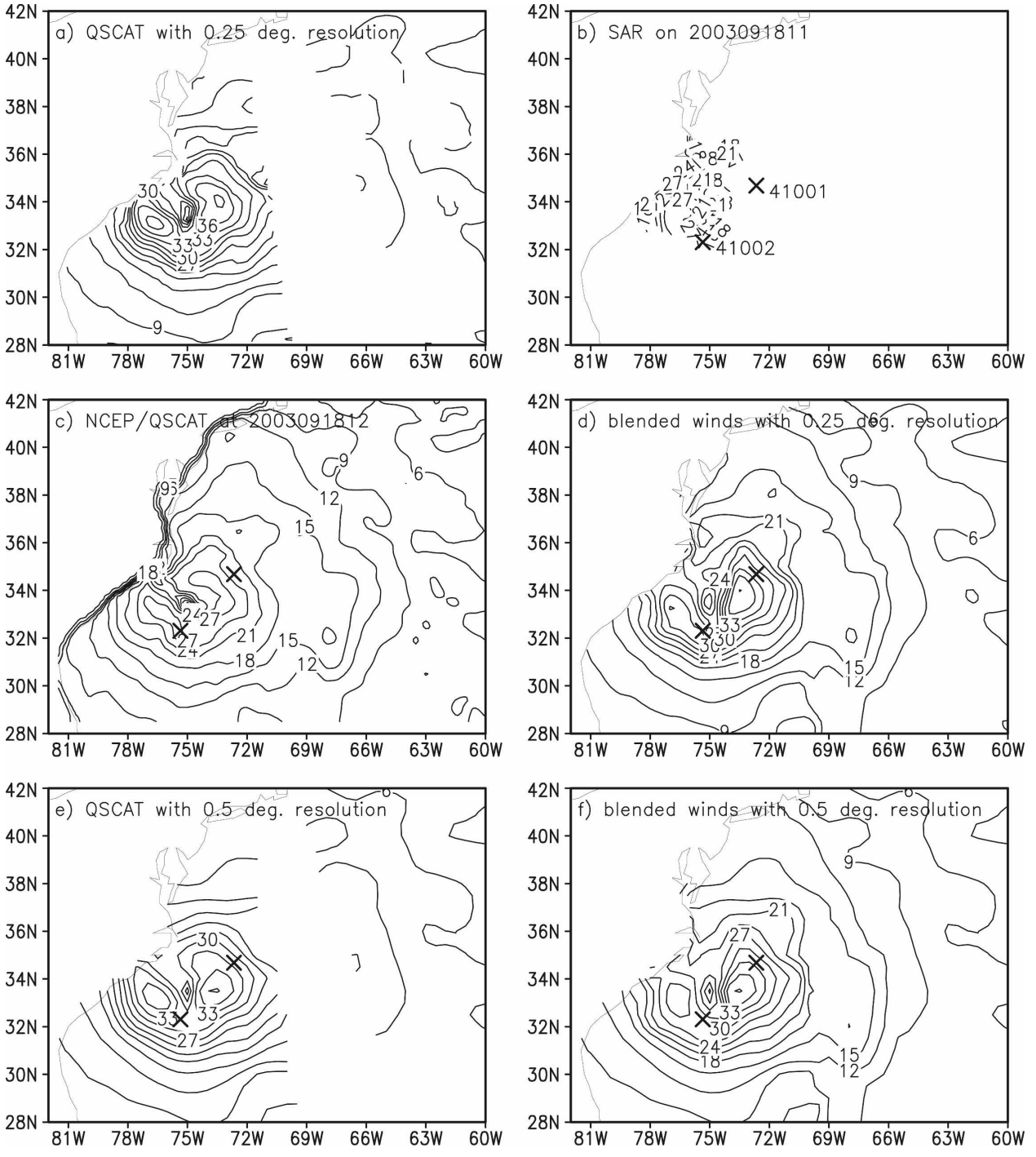

FIG. 4. Wind field comparison showing (a) winds (m s^{-1}) from QuikSCAT data for swaths during the period from 0600 to 1800 UTC 18 Sep 2003 at 0.25° resolution, (b) an SAR image at 1100 UTC 18 Sep, (c) QSCAT–NCEP winds with 0.5° resolution, used as background data to fill gaps between QuikSCAT swaths, (d) blended winds with 0.25° resolution, (e) QuikSCAT winds from 0600 to 1800 UTC 18 Sep 2003 at 0.5° resolution, and (f) blended winds with 0.5° resolution. Buoy 41001 is at (34.683°N, 72.662°W), and buoy 41002 is at (32.31°N, 75.35°W).

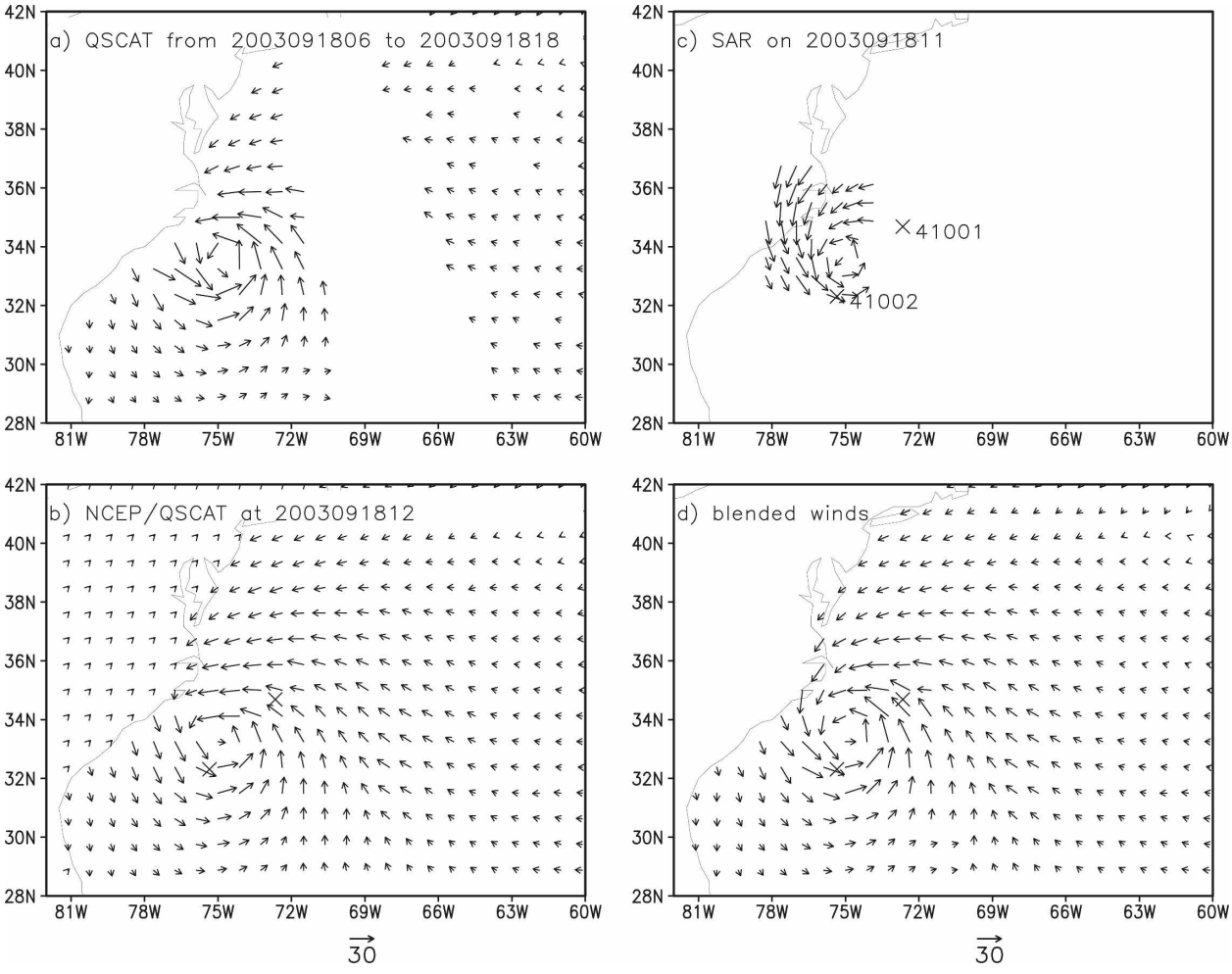

FIG. 5. As in Fig. 2, but showing vector winds: speed (m s^{-1}) and direction.

A butterfly shape is evident in the blended winds, and in both the QuikSCAT winds as well as the blended QSCAT–NCEP winds, but it is not present in the SAR-derived winds. Some of the butterfly shape comes from QSCAT issues with azimuth and polarization-dependent rain contamination and possibly also through ambiguity selection. Some of these features appear to be real, based on data from areas that are unlikely to be seriously biased by rain. At this time, it is not possible to assess how much is real and how much is rain related because we do not have appropriate comparison data. This is an issue that is worthy of additional study.

Table 2 compares wind speed measurements at buoys 41001 and 41002 with SAR, QSCAT–NCEP, and the blended winds. For winds in excess of 20 m s^{-1}, the buoy-related biases from buoys 41001 and 41002 are assumed not to constitute a dominant effect in terms of accounting for the difference between our final winds and the buoy data for the SAR image at 1100 UTC 18 Sep 2003 in Table 2. As discussed in section 3, rain flagging is a concern, as it is different in the blended product (MC2–QSCAT) than in the QSCAT–NCEP winds. Specifically, QSCAT–NCEP winds would allow more rain-contaminated winds to be used in high-wind

TABLE 2. Comparison of wind speed (m s^{-1}) at buoys 41001 and 41002, with SAR, QSCAT–NCEP, and our new blended winds applying the variational method.

Locations/source	Buoy	SAR	QSCAT–NCEP	New blended winds
SAR image at 1100 UTC 18 Sep 2003				
41001	21.31	Missing	23.2	29.10
41002	24.79	24	27.5	24.68
SAR image at 2300 UTC 17 Sep 2003				
41001	19	Missing	22.6	22.88
41002	22.85	Missing	24.9	30.3

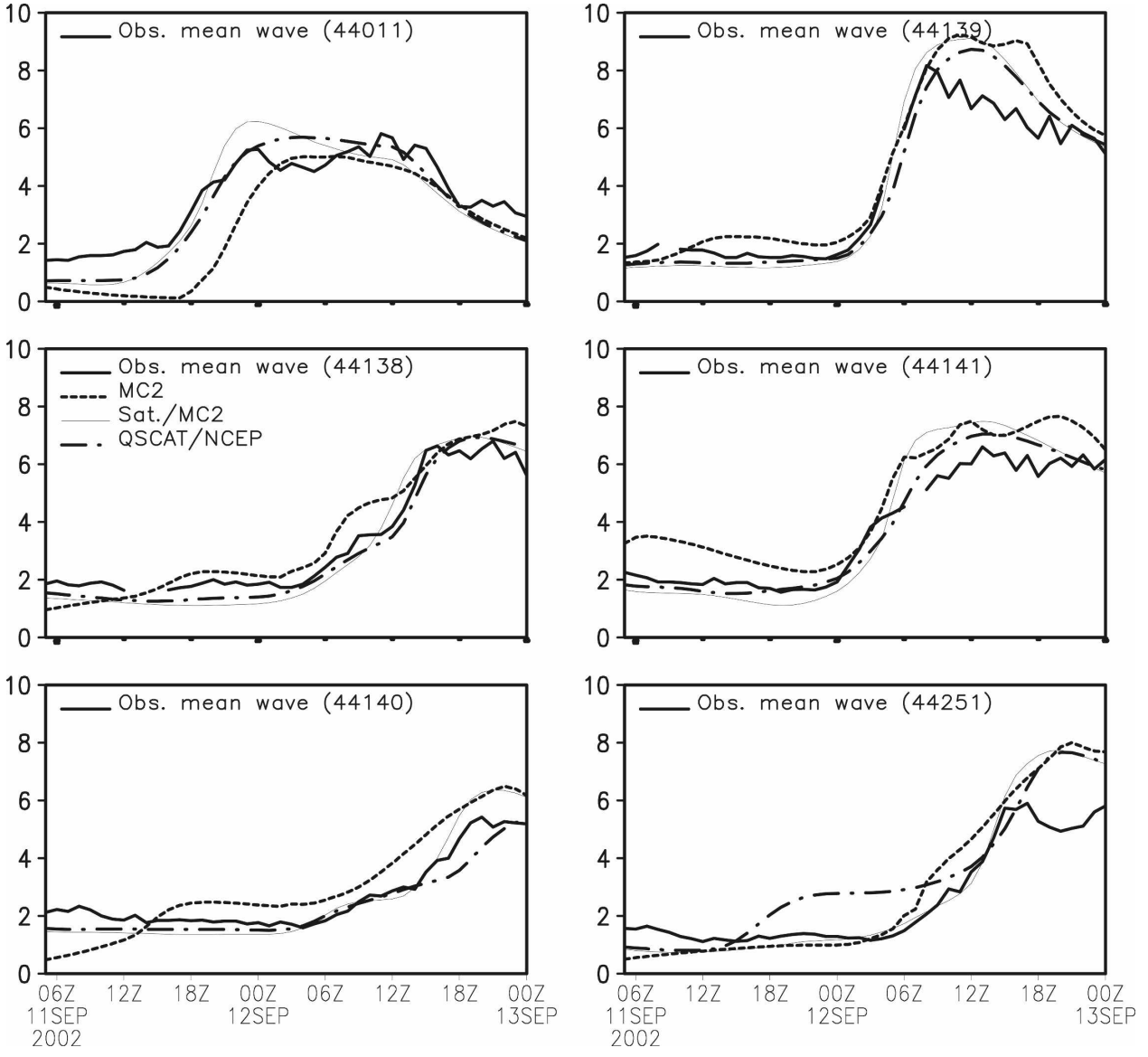

FIG. 6. As in Fig. 2, but for SWH (m).

situations (exceeding 15 m s^{-1} or so) than would occur in MC2–QSCAT winds. The difference in rain flagging is suggested as a factor in the results. Moreover, very high winds from the blending could result from the curl constraint in the variational method we applied—sometimes the shear is changed as the variational method attempts to match the changes in the background curl. Last, accepted error bars are 2 m s^{-1} or 10% for SAR wind speeds below 20 m s^{-1}. For higher winds typical of hurricanes, the CMOD5 algorithm saturates and small changes of sigma from 0 of 0.5 dB can potentially cause errors in the range of 10–20 m s^{-1}. Therefore, CMOD5 may need to be tuned in intense storm cases because of radar-backscattered cross-section (NRCS) saturation during high winds. However, the data for the SAR image at 1100 UTC 18 September 2003 in Table 2 show that our SAR and buoy estimates are comparable; the SAR estimate is 24 m s^{-1} while the buoy suggests 24.79 m s^{-1}, although no tuning is done in this study.

An earlier SAR image acquired at 2300 UTC 17 September also captured Isabel's eye. In applying our variational method, the same issues remain. Overall, for the two SAR images of Isabel, our final blended winds tend to be biased high relative to buoy and QSCAT–NCEP blended winds, as shown in Table 2. However, NHC estimates for maximum peak winds are 46 m s^{-1} for these two SAR images, which is still higher

TABLE 3. As in Table 1, but for SWH, for correlation coefficients and RMSE comparing observations with simulated SWH, as driven by 10-m winds from the uncoupled MC2 control simulation, the blended Sat–MC2 wind, and the blended QSCAT–NCEP wind.

Buoy	44011	44138	44139	44140	44141	44251
			Correlation coef			
MC2	0.8949	0.9662	0.9686	0.8991	0.9754	0.9692
Sat–MC2	0.9326	0.9898	0.9859	0.9854	0.9705	0.9728
QSCAT–NCEP	0.9611	0.9897	0.9754	0.9631	0.9840	0.9046
			RMSE			
MC2	1.3721	0.6911	1.7270	0.9544	1.1289	1.1812
Sat–MC2	0.8612	0.5911	0.9322	0.5757	0.9134	1.0513
QSCAT–NCEP	0.7181	0.4550	0.7957	0.4606	0.5241	1.2713

than the maxima for either of our blended wind field estimates.

6. Upper-ocean fields

For Gustav, results for simulated and observed significant wave heights (SWH) are shown in Fig. 6. These results suggest that wave model estimates, driven by our blended Sat–MC2 winds, compare favorably to wave results from baseline MC2 winds, or with QSCAT–NCEP winds. Statistical measures of improvement are given in Table 3. Averaged over the buoys, our blended Sat–MC2 winds result in waves with an RMSE of 0.82 m, which is similar to 0.71 m for QSCAT–NCEP and somewhat lower than 1.18 m for baseline MC2 winds. However, the wave model results in Table 3 seem inconsistent with the wind results in Table 1, where Sat–MC2 winds were shown to be slightly better than QSCAT–NCEP winds. This outcome may be explained by noting (section 5a) that, whereas Figs. 1a and 1b suggest that maximum winds from Sat–MC2 are more comparable to NHC winds than to QSCAT–NCEP winds, the buoys are outside the maximum wind area and differences between the QSCAT–NCEP and Sat–MC2 winds are small. Moreover, Fig. 3c shows that during Gustav's peak, the difference in Sat–MC2 winds *minus* QSCAT–NCEP winds is large ($\sim$12 m s^{-1}) and occurs in a region to the south

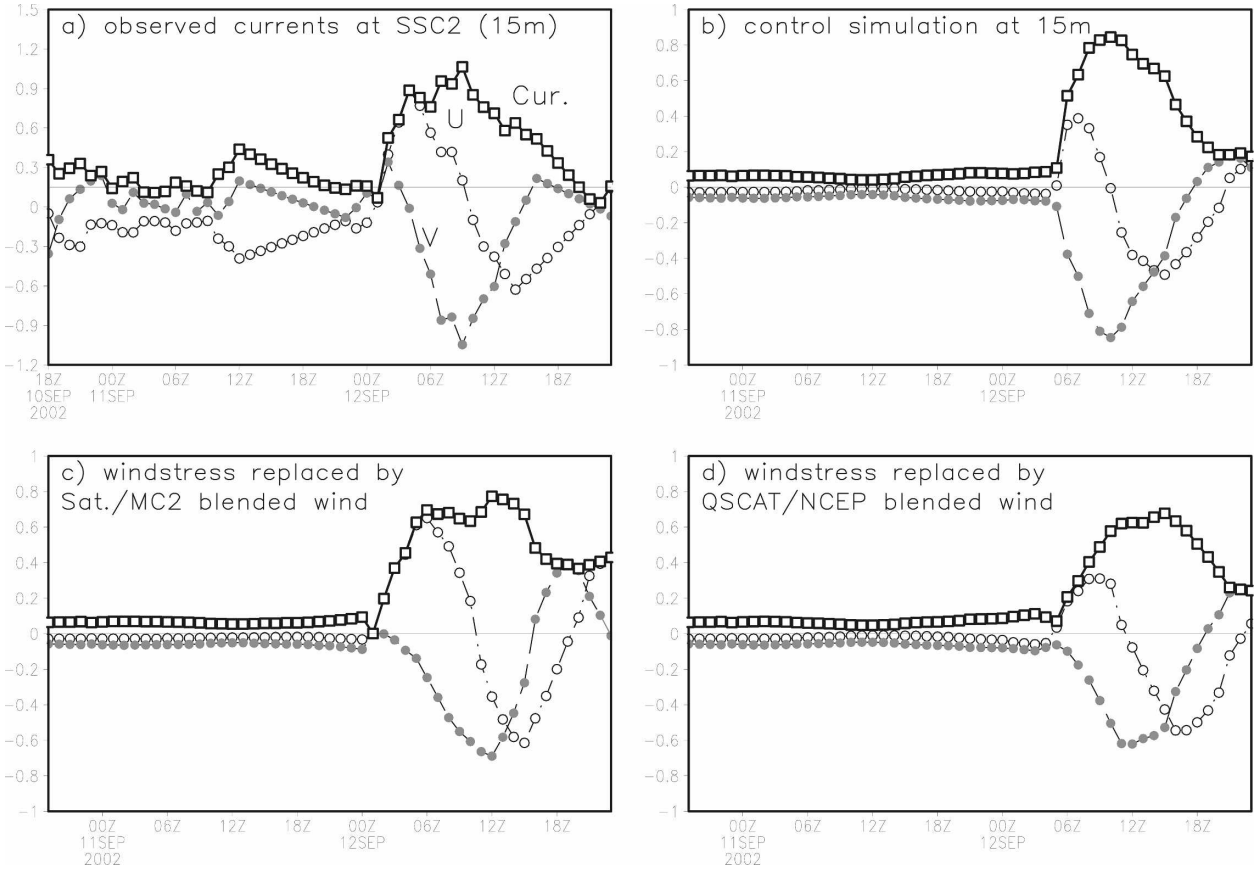

FIG. 7. Comparison of currents at 15 m including total current (open squares) and U (open circles) and V (filled circles) components (m s^{-1}): (a) observations at the SSC2 location, (b) baseline control POM driven by MC2 winds, (c) POM results using blended Sat–MC2 winds, and (d) POM results using QSCAT–NCEP winds.

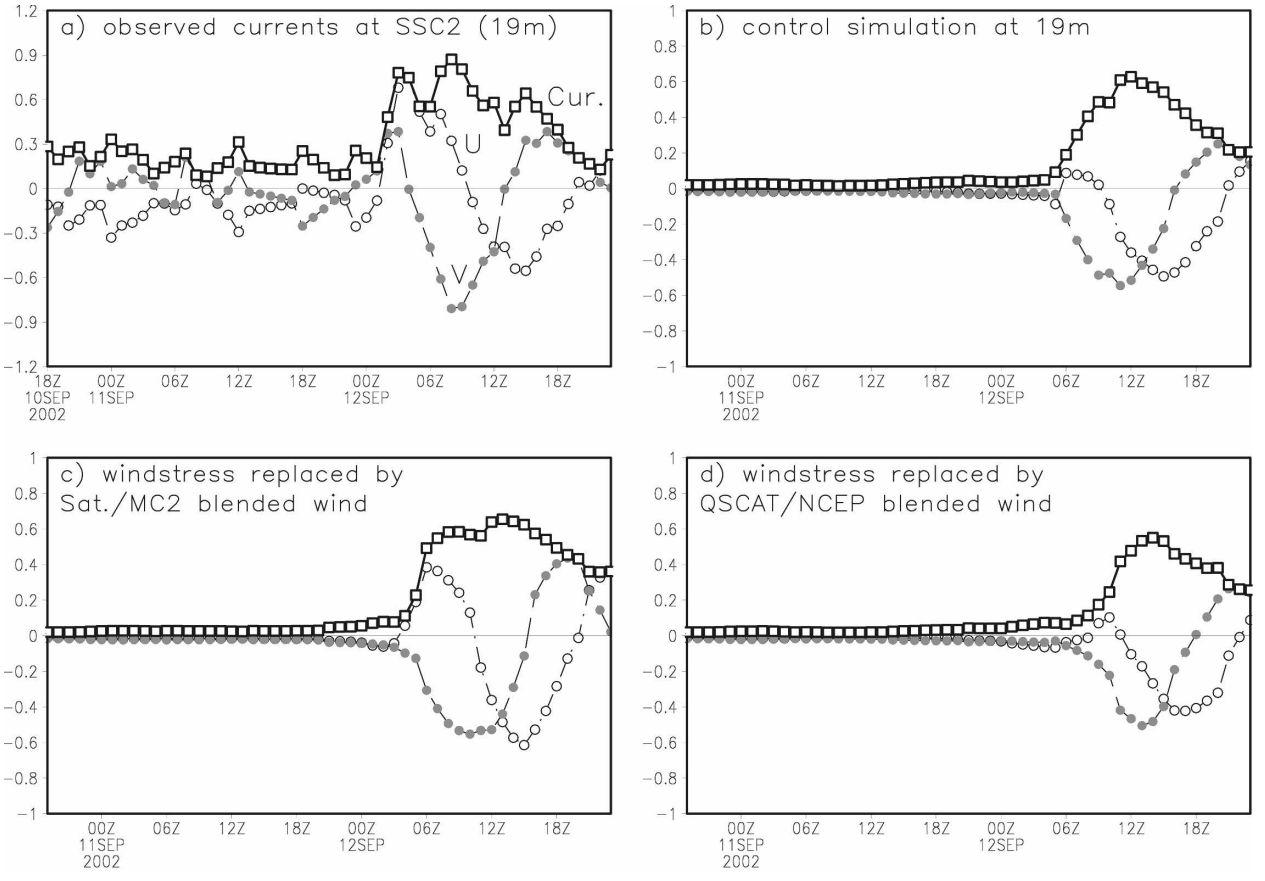

FIG. 8. As in Fig. 7, but for currents at 19-m depth.

of the buoys. A slight overestimate in Sat–MC2 wind in the high-wind region of the storm (suggested in Figs. 1b and 3c) generates excess wave energy that propagates outward from the storm center and shows up in the buoy wave time series measurements in Table 3.

Results for upper-ocean currents at 15- and 19-m depths are given in Figs. 7 and 8, respectively, using a one-way forcing formulation whereby atmospheric fields are used to drive POM and there is no feedback (Perrie et al. 2004). Observations suggest that a tidal periodicity is present in these data, on the order of ~6 h, which is not included in the simulations. In POM simulations using baseline MC2 winds (Figs. 7b and 8b), as well as those using our Sat–MC2 winds (Figs. 7c and 8c) and QSCAT–NCEP winds (Figs. 7d and 8d), the arrival of the storm is obvious, beginning at 0600 UTC 12 September and coinciding well with the observed data. The overall model performance resulting from the Sat–MC2 winds compares favorably to that of either the MC2 winds or the QSCAT–NCEP winds, as shown in Table 4. Relative to the observed data at 15-m depth, our Sat–MC2 winds result in RMSE (U, V) components of (0.20, 0.32) cm s^{-1}, as compared with (0.30, 0.29) cm s^{-1} for baseline MC2 winds, and (0.36, 0.42) cm s^{-1} for QSCAT–NCEP winds. Correspondingly, at 19-m depth, our RMSE values are (0.26, 0.21) cm s^{-1}, as compared with (0.30, 0.23) cm s^{-1} for baseline MC2 winds and (0.35, 0.35) cm s^{-1} for QSCAT–NCEP winds.

TABLE 4. Correlation coefficients and RMSEs for current components (U, V) between the observations and the baseline MC2 simulation, the blended Sat–MC2 wind, and the QSCAT–NCEP wind.

	U		*V*	
Obs	Correlation coef	RMSE	Correlation coef	RMSE
	Obs at 15-m depth			
MC2	0.7611	0.3036	0.7015	0.2889
Sat–MC2	0.8958	0.2002	0.6448	0.3207
QSCAT–NCEP	0.6126	0.3567	0.1979	0.4208
	Obs at 19-m depth			
MC2	0.7492	0.3032	0.9173	0.2284
Sat–MC2	0.7341	0.2641	0.8647	0.2088
QSCAT–NCEP	0.6903	0.3521	0.4449	0.3452

7. Conclusions

We have conducted a study of marine winds for Hurricanes Gustav and Isabel. We have constructed enhanced wind fields using a variational data assimilation method to blend remotely sensed data with background wind fields. The variational approach follows those of Pegion et al. (2000), O'Brien and Bourassa (2003), Bourassa et al. (2002), and Morey et al. (2005). We have shown that our enhanced winds compare well to NHC analysis winds in Hurricanes Gustav and Isabel.

At the peak of Gustav, our enhanced winds can reduce the QSCAT–NCEP wind bias by about 10 m s^{-1} relative to NHC winds. With respect to in situ buoy winds in Gustav, we show that our enhanced winds have an average RMSE of 1.89 m s^{-1}, which is about 39% better than baseline MC2 winds and somewhat (about 27%) better than QSCAT–NCEP blended winds. Analysis of Hurricane Isabel focused on the two SAR images that captured Isabel's eye. We applied our variational method to assimilate the SAR-observed data, which suggested new information for the central portion of Isabel. The resulting blended winds are similar to QSCAT–NCEP winds in comparisons with buoy winds. However, rain flagging is a concern for either of the wind fields.

In our study of Hurricane Gustav, resultant winds were used to drive wave and ocean current models. Wave and ocean current simulation results compare relatively well to in situ observed data. In the storms that were considered, in terms of SWH *wave* simulations, our enhanced winds result in an *average* RMSE of 0.82 m, which is about 28% better than results for baseline MC2 winds and is similar to results from QSCAT–NCEP winds. Relative to observed currents at 15 and 19 m, our blended Sat–MC2 winds result in about a 40% improvement in RMSE values for (U, V) components, when compared with results from QSCAT–NCEP winds.

Acknowledgments. We thank John Loder and Yuri Geselin for providing data from the BIO ocean moorings at SSC2. We thank Youyu Lu and Bash Toulany for discussions in using POM and WW3, respectively. Funding was provided by the Panel on Energy Research and Development, the Canada Foundation for Atmospheric and Climate Studies, the Natural Science and Engineering Research Council, C-SOLAS, NASA OVWST, and the SURA SCOOP program.

REFERENCES

Alpers, W., and C. Melsheimer, 2004: Rainfall. *Synthetic Aperture Radar Marine User's Manual,* C. R. Jackson and J. R. Apel, Eds., NOAA/NESDIS/OAR, 355–371. [Available online at http://www.sarusersmanual.com.]

Bender, M. A., and I. Ginis, 2000: Real-case simulations of hurricane–ocean interaction using a high-resolution coupled model: Effects on hurricane intensity. *Mon. Wea. Rev.,* **128,** 917–946.

Benoit, R., M. Desgagne, P. Pellerin, Y. Chartier, and S. Desjardins, 1997: The Canadian MC2: A semi-implicit semi-Lagrangian wide-band atmospheric model suited for fine-scale process studies and simulation. *Mon. Wea. Rev.,* **125,** 2382–2415.

Bourassa, M. A., R. S. Shawn, and J. O. James, 2002: Assimilation of scatterometer and in situ winds for regularly gridded products. Preprints, *Sixth Symp. on Integrated Observing Systems,* Orlando, FL, Amer. Meteor. Soc., 13–18.

——, D. M. Legler, J. J. O'Brien, and S. R. Smith, 2003: SeaWinds validation with research vessels. *J. Geophys. Res.,* **108,** 3019, doi:10.1029/2001JC001081.

——, R. Romero, S. R. Smith, and J. J. O'Brien, 2005: A new FSU winds climatology. *J. Climate,* **18,** 3692–3704.

Chin, T. M., R. F. Milliff, and W. G. Large, 1998: Basin-scale high-wavenumber sea surface wind fields from multiresolution analysis of scatterometer data. *J. Atmos. Oceanic Technol.,* **15,** 741–763.

Draper, D. W., and D. G. Long, 2004: Simultaneous wind and rain retrieval using SeaWinds data. *IEEE Trans. Geosci. Remote Sens.,* **42,** 1411–1423.

Ebuchi, E., H. C. Graber, and M. J. Caruso, 2002: Evaluation of wind vectors observed by QuikSCAT/SeaWinds using ocean buoy data. *J. Atmos. Oceanic Technol.,* **19,** 2049–2062.

Hersbach, H., 2003: CMOD5—An improved geophysical model function for ERS C-band scatterometry. ECMWF Tech. Memo. 395, 50 pp.

Horstmann, J., D. R. Thompson, F. Monaldo, H. C. Graber, and S. Iris, 2005: Can synthetic aperture radars be used to estimate hurricane force winds? *Geophys. Res. Lett.,* **32,** L22801, doi:10.109/2005GL023992.

Kain, J. S., and J. M. Fritsch, 1993: Convective parameterization for mesoscale models: The Kain–Fritsch scheme. *The Representation of Cumulus Convection in Numerical Models, Meteor. Monogr.,* No. 46, Amer. Meteor. Soc., 165–170.

Mellor, G. L., 1998: User's guide for a three-dimensional primitive equation numerical ocean model. Program in Atmospheric and Oceanic Sciences, Princeton University, 35 pp. [Available online at http://www.aos.princeton.edu/WWWPUBLIC/htdocs.pom.]

Moon, I.-J., I. Ginis, T. Hara, H. L. Tolman, C. W. Wright, and E. J. Walsh, 2003: Numerical simulation of sea surface directional wave spectra under hurricane wind forcing. *J. Phys. Oceanogr.,* **33,** 1680–1706.

Morey, S. L., M. A. Bourassa, X. Davis, J. J. O'Brien, and J. Zavala-Hidalgo, 2005: Remotely sensed winds for forcing ocean models. *J. Geophys. Res.,* **110,** C10024, doi:10.1029/2004JC002338.

——, S. Baig, M. A. Bourassa, D. S. Dukhovskoy, and J. J. O'Brien, 2006: Remote forcing contribution to storm-induced sea level rise during Hurricane Dennis. *Geophys. Res. Lett.,* **33,** L19603, doi:10.1029/2006GL027021.

Mouche, A., D. Hauser, and V. Kudryavtsev, 2006: Radar scattering of the ocean surface and sea-roughness properties: A combined analysis from dual-polarizations airborne radar observations and models in C band. *J. Geophys. Res.,* **111,** C09004, doi:10.1029/2005JC003166.

O'Brien, J. J., and M. Bourassa, 2003: The best winds for ocean models? Preprints, *12th Conf. on Interactions of the Sea and Atmosphere and 12th Conf. on Satellite Meteorology and Oceanography,* Long Beach, CA, Amer. Meteor. Soc., J2.1.

Pegion, P. J., M. A. Bourassa, D. M. Legler, and J. J. O'Brien, 2000: Objectively derived daily "winds" from satellite scatterometer data. *Mon. Wea. Rev.,* **128,** 3150–3168.

Perrie, W., X. Ren, W. Zhang, and Z. Long, 2004: Simulation of extratropical Hurricane Gustav using a coupled atmosphere–ocean–sea spray model. *Geophys. Res. Lett.,* **31,** L03110, doi:1029/2003GL018571.

Powell, M. D., S. H. Houston, L. R. Amat, and N. Morisseau-Leroy, 1998: The HRD real-time hurricane wind analysis system. *J. Wind Eng. Indust. Aerodyn.,* **77/78,** 53–64.

Shen, H., W. Perrie, and Y. He, 2006: A new hurricane wind retrieval algorithm for SAR images. *Geophys. Res. Lett.,* **33,** L21812, doi:10.1029/2006GL027087.

Thompson, D. R., T. M. Elfouhaily, and B. Chapron, 1998: Polarization ratio for microwave backscatter from ocean surface at low to moderate incidence angles. *Proc. Int. Geoscience and Remote Sensing Symp.,* Vol. III, Seattle, WA, IEEE, 1671–1673.

Tolman, H. L., 2002: User manual and system documentation of WAVEWATCH-III version 2.22. Tech. Note 222, 133 pp. [Available online at http://polar.ncep.noaa.gov/waves.]

——, L. Balasubramaniyan, L. D. Burroughs, D. V. Chalikov, Y. Y. Chao, H. S. Chen, and V. M. Gerald, 2002: Development and implementation of wind-generated ocean surface wave models at NCEP. *Wea. Forecasting,* **17,** 311–333.

Vachon, P., and F. Dobson, 2000: Wind retrieval from Radarsat SAR images: Selection of a suitable C-band HH polarization wind model. *Can. J. Remote Sens.,* **26,** 306–313.

Weissman, D. E., M. A. Bourassa, and J. Tongue, 2002: Effects of rain rate and wind magnitude on SeaWinds scatterometer wind speed errors. *J. Atmos. Oceanic Technol.,* **19,** 738–746.

Xu, F., W. Perrie, B. Toulany, and P. C. Smith, 2007: Wind-generated waves in Hurricane Juan. *Ocean Modell.,* **16,** 188–205.